



Multiple Solutions for Slip Effects on Dissipative Magneto-Nanofluid Transport Phenomena in Porous Media: Stability Analysis

Yogesh Gupta¹, Puneet Rana¹, Osman Anwar Bég², Ali Kadir³

¹Assistant Professor, Department of Mathematics, Jaypee Institute of Information Technology, A-10, Sector-62, Noida-201307, Uttar Pradesh, India, Email(s): yogesh.gupta@jiit.ac.in, puneet.rana@jiit.ac.in

²Professor, Aeronautical and Mechanical Engineering, School of Computing, Science & Engineering, University of Salford, Newton Building, M54WT, UK. Email: o.a.beg@salford.ac.uk

³Senior Lecturer, Petroleum and Gas Engineering, School of Computing, Science & Engineering, University of Salford, Newton Building, M54WT, UK. Email: a.kadir@salford.ac.uk

Received June 30 2019; Revised August 08 2019; Accepted for publication August 09 2019.

Corresponding author: Puneet Rana (puneet.rana@jiit.ac.in, puneetranaiitr@gmail.com)

© 2020 Published by Shahid Chamran University of Ahvaz

& International Research Center for Mathematics & Mechanics of Complex Systems (M&MoCS)

Abstract. In the present paper, a numerical investigation of transport phenomena is considered in electrically-conducting nanofluid flow within a porous bed utilizing Buongiorno's transport model and *Runge-Kutta-Fehlberg fourth-fifth* order method. Induced flow by non-isothermal stretching/shrinking sheet along with magnetic field impact, dissipation effect, and slip conditions at the surface are also included. The numerical results show the existence of two branches of the solution for a selected range of the governing parameters. The physical significance of both branches of solutions is ensured by performing a stability analysis in which a linearized eigenvalue problem is solved. The multiple regression analysis with the help of MATLAB *LinearModel.fit* package has also been conducted to estimate the dependence of the parameters on Nusselt number.

Keywords: MHD, Nanofluid, Shrinking sheet, Dual solutions, Porous medium, Eigenvalues.

1. Introduction

Motivated by many industrial applications such as in materials and polymer processing, in the manufacturing of glass sheets and paper, in textile industries and many others, stretching and shrinking surfaces have gained so much interest among researchers. An early analysis of boundary layer flow over a stretching surface was presented by Crane [1]. In recent years, much attention has been paid to investigate fluid flow over a *shrinking* surface [2]. Fang [3] has studied the boundary layer flow over a nonlinear shrinking sheet. Fang and Zhang [4] derived exact solutions for magneto-hydrodynamic flow over a shrinking sheet and investigated the range of magnetic field and suction parameters for the existence of the solutions whereas nonlinear study has been reported by Javed *et al.* [5]. The work has been extended to nanofluid after 2006 when the Buongiorno [6] formulated a new mathematical model for study transport phenomena in nanofluids. The extension has been reported by Rohni *et al.* [7], Zaimi *et al.* [8], Naramgari and Sulochana [9] on nanoparticle effects on shrinking sheet problem.

The no-slip boundary conditions are sometimes unrealistic and the above sources utilized the no-slip condition. However, partial slip between the fluid and moving surface (stretching/shrinking) sheet should not be neglected in case of nanoparticles. Uddin *et al.* [10] have investigated slip flow induced by a nanofluid sheet along with the impact of thermal radiation. Singh and Chamkha [11] analyzed vertical shrinking sheet with consideration of second-order slip.

Many researchers have extended this work to nanofluid for various configurations utilizing the magnetic field (Hsiao [12-15], Waqas *et al.* [16-17], Dhanai [18]), non-Newtonian base fluid (Rao *et al.*[19], Siavashi *et al.* [20], Dhanai *et al.*[21]), porous media (Izadi *et al.*[22], Bég *et al.*[23]), Entropy generation minimization (Rashid *et al.* [24], Khan *et al.* [25], Shukla *et al.* [26], Rana *et al.* [27], Rana *et al.* [28]) and the other possible extensions *i.e.* in Cattaneo-Christov (CC) heat flux with variable boundary layer thickness, heat source/sink and chemical reaction [29-33].

A new branch of the solution is reported in different boundary layer flow problem especially in shrinking surfaces with suction and non-unique solutions have been documented to specific ranges of governing parameters. Considering the slip effects, Ghosh *et al.* [34] and Rana *et al.* [35] reported the two branches of the solution with suction parameter without and with nanoparticles respectively. In porous, Merkin [36] studied the mixed convection and revealed the existence of multiple branches which later extended with slip conditions and Brinkman model assumption by Harris *et al.* [37]. The critical points (turning points) along with multiple solutions and stability analysis is investigated in different problems numerically using MATLAB building bvp4c solver (Awaludin *et al.* [38], Yasin *et al.* [39]) RKF-shooting method (Rana *et al.* [40-41]), homotopy analysis method (Rana *et al.* [42-43]) *etc.* The stability of results by constructing the eigenvalue problem predicts the physical realizable upper branch and non-realizable lower branch.

To the author’s best of knowledge, the present study which predicts the multiple solutions in transport phenomena of electrically-conducting nanofluid over a permeable shrinking sheet in a porous medium with partial slip has not been reported so far. The stability analysis for physical realizable branch and regression analysis (stable branch) is also performed. Multiple Regression Analysis (MRE) with the goodness of fit, is also shown for the upper branch for different sets of parameters.

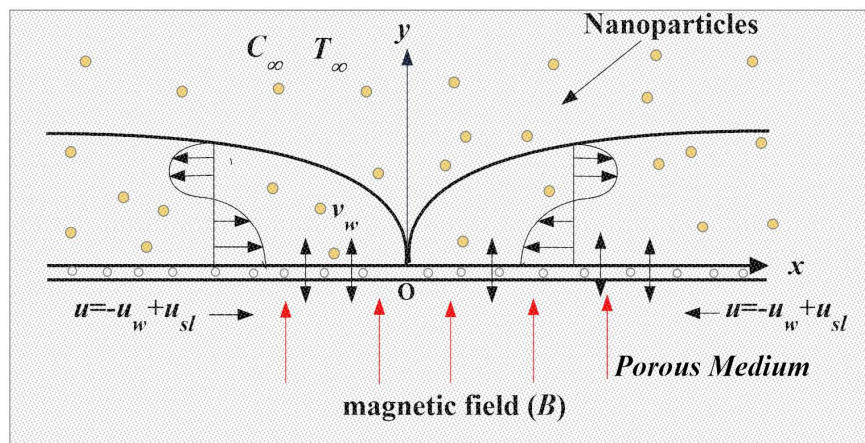


Fig. 1. Physical model and coordinate system

2. Nanofluid Modeling

Buongiorno’s nanofluid 2D flow model for uniform porous bed is considered with flow induced by a permeable stretching/shrinking sheet taken along the x -axis (Fig. 1). The sheet shrinks with linear velocity $\tilde{u}_w = \chi U$ and $U = a\tilde{x}$ where a is positive constant and $\chi = \pm 1$ (stretching/shrinking). The wall mass transfer velocity is v_w , such that only suction ($v_w < 0$) is considered here. A uniform magnetic field B is assumed to be imposed transverse to the plane of the hot sheet having a temperature of $T_w = T_\infty + A\tilde{x}^2$ and $T_\infty = D\tilde{x}^2$ is the temperature at the free stream where A and D are constant. Nanoparticle concentration at the sheet is controlled by a new revised boundary condition [18]. Darcy’s law with viscous dissipative heat is employed for the porous medium. Under these assumptions, the boundary layer equations may be written following [19]-[21] as:

$$\frac{\partial \tilde{u}}{\partial \tilde{x}} + \frac{\partial \tilde{v}}{\partial \tilde{y}} = 0 \tag{1}$$

$$\tilde{u} \frac{\partial \tilde{u}}{\partial \tilde{x}} + \tilde{v} \frac{\partial \tilde{u}}{\partial \tilde{y}} = v_{nf} \frac{\partial^2 \tilde{u}}{\partial \tilde{y}^2} - \left(\frac{\sigma_{nf} B^2}{\rho_{nf}} + \frac{\mu_e}{\rho_{nf} k_e} \right) \tilde{u} \tag{2}$$

$$(\rho c)_{nf} \left(\tilde{u} \frac{\partial \tilde{T}}{\partial \tilde{x}} + \tilde{v} \frac{\partial \tilde{T}}{\partial \tilde{y}} \right) = k_{nf} \frac{\partial^2 \tilde{T}}{\partial \tilde{y}^2} + (\rho c)_p \left(D_B \left(\frac{\partial \tilde{C}}{\partial \tilde{y}} \right) + \frac{D_T}{T_\infty} \left(\frac{\partial \tilde{T}}{\partial \tilde{y}} \right) \right) \left(\frac{\partial \tilde{T}}{\partial \tilde{y}} \right) + \frac{\mu_e}{k_e} \tilde{u}^2 + \mu_{nf} \left[\frac{\partial \tilde{u}}{\partial \tilde{y}} \right]^2 \tag{3}$$

$$\tilde{u} \frac{\partial \tilde{C}}{\partial \tilde{x}} + \tilde{v} \frac{\partial \tilde{C}}{\partial \tilde{y}} = D_B \frac{\partial^2 \tilde{C}}{\partial \tilde{y}^2} + \frac{D_T}{T_\infty} \frac{\partial^2 \tilde{T}}{\partial \tilde{y}^2} \tag{4}$$

The imposed boundary conditions at the wall (sheet) and freestream are:

$$\tilde{u} = -\tilde{u}_w + \tilde{u}_{sl}, \quad \tilde{v} = \tilde{v}_w, \quad \tilde{T} = \tilde{T}_w + \tilde{T}_{sl}, \quad D_B \frac{\partial \tilde{C}}{\partial \tilde{y}} + \frac{D_T}{T_\infty} \frac{\partial \tilde{T}}{\partial \tilde{y}} = 0 \quad \text{at } \tilde{y} = 0 \tag{5a}$$

$$\tilde{u} = 0, \quad \tilde{v} = 0, \quad \tilde{T} = \tilde{T}_\infty, \quad \tilde{C} = \tilde{C}_\infty \quad \text{as } \tilde{y} \rightarrow \infty \tag{5b}$$

where \tilde{u} and \tilde{v} are the velocity components in the \tilde{x} and \tilde{y} -directions respectively, subscript nf is for nanofluids, the rest parameters have their usual meanings.

$$\eta = \tilde{y} \sqrt{\frac{a}{\nu_{nf}}}, \quad \tilde{u} = a f'(\eta), \quad \tilde{v} = -\sqrt{a \nu_{nf}} f(\eta), \quad \theta(\eta) = \frac{\tilde{T} - \tilde{T}_\infty}{\tilde{T}_w - \tilde{T}_\infty}, \quad \phi(\eta) = \frac{\tilde{C} - \tilde{C}_\infty}{\tilde{C}_w - \tilde{C}_\infty} \tag{6}$$

Equation (1) is thereby satisfied automatically and the governing Eqs. (2)-(4) transform to the following system of coupled, nonlinear, ordinary differential equations:

$$\frac{d^3 f}{d\eta^3} + f \frac{d^2 f}{d\eta^2} - \left(\frac{df}{d\eta} + (M^2 + P_e) \right) \frac{df}{d\eta} = 0 \tag{7}$$

$$\frac{1}{Pr} \left(\frac{d^2 \theta}{d\eta^2} + Nb \frac{d\theta}{d\eta} \frac{df}{d\eta} + Nt \left(\frac{d\theta}{d\eta} \right)^2 \right) + f \frac{d\theta}{d\eta} - 2 \frac{df}{d\eta} \theta + Ec \left(\left(\frac{d^2 f}{d\eta^2} \right)^2 + P_e \left(\frac{df}{d\eta} \right)^2 \right) = 0 \tag{8}$$

$$\frac{d^2 \phi}{d\eta^2} + Scf \frac{d\phi}{d\eta} + \frac{Nt}{Nb} \frac{d^2 \theta}{d\eta^2} = 0 \tag{9}$$

The transformed boundary conditions assume the form:

$$f(0) = \beta, \quad \left. \frac{df}{d\eta} \right|_{\eta=0} = \chi + \lambda \left. \frac{d^2 f}{d\eta^2} \right|_{\eta=0}, \quad \theta(0) = 1 + \delta \left. \frac{d\theta}{d\eta} \right|_{\eta=0}, \quad Nb \left. \frac{d\phi}{d\eta} \right|_{\eta=0} + Nt \left. \frac{d\theta}{d\eta} \right|_{\eta=0} = 0, \tag{10}$$

$$\left. \frac{df}{d\eta} \right|_{\eta \rightarrow \infty} = 0, \quad \theta(\eta)|_{\eta \rightarrow \infty} = 0, \quad \phi(\eta)|_{\eta \rightarrow \infty} = 0$$

Here prime denotes the differentiation with respect to η only and the emerging dimensionless thermo-physical parameters are defined as follows:

$M = \sqrt{\sigma_{nf} B^2 / a \rho_{nf}}$ (magnetic field parameter), $P_e = \mu_e / a \rho_{nf} k_e$ (permeability parameter), $Pr = \nu_{nf} / \alpha_{nf}$ (Prandtl number), $Sc = \nu_{nf} / D_B$ (Schmidt number), $Ec = a^2 / cA$ (Eckert number), $Nb = (\rho c)_p D_B C_\infty / (\rho c)_{nf} \alpha_{nf}$ (Brownian motion parameter), $Nt = (\rho c)_p D_T (\tilde{T}_w - \tilde{T}_\infty) / (\rho c)_{nf} \alpha_{nf} \tilde{T}_\infty$ (thermophoresis parameter), $\beta = -v_w / \sqrt{a \nu_{nf}}$ (wall mass transfer parameter), $\lambda = L_1 \sqrt{a / \nu_{nf}}$ (velocity slip parameter), $\delta = L_2 \sqrt{a / \nu_{nf}}$ (thermal slip parameter).

The important physical quantities are skin friction C_f and local Nusselt number Nu_x which are defined as follows:

$$C_f Re_x^{1/2} = f''(0), \quad \frac{Nu_x}{Re_x^{1/2}} = -\theta'(0) \tag{11}$$

where $Re_x = u_w \tilde{x} / \nu_{nf}$ is local Reynolds number.

The closed-form analytical solution of Eq. (7) (shrinking sheet) can be assumed to be a form of $f(\eta) = A + B \exp(-C\eta)$ using the first three boundary conditions of Eq. (10). After substituting this relation in Eq. (7), we get $A = \beta - B$, $B = 1 / (C + \lambda C^2)$ where the value of C can be obtained from the positive roots of the following cubic equation,

$$\lambda C^3 + (1 - \beta \lambda) C^2 - (\beta + \lambda(M^2 + P_e)) C + 1 - M^2 - P_e = 0 \tag{12}$$

Without slip conditions ($\lambda = 0$), the above equation takes quadratic form and the solution is given by:

$$C = \frac{\beta \pm \sqrt{\beta^2 - 4(1 - M^2 - P_e)}}{2} \quad \text{which } \beta^2 > 4(1 - M^2 - P_e) \text{ for multiple solutions}$$

If $\beta^2 < 4(1 - M^2 - P_e)$ then there will be no solution and unique solution for $\beta^2 = 4(1 - M^2 - P_e)$. Hence, the exact solution takes the following form:

$$f(\eta) = \beta - \frac{1}{\frac{\beta \pm \sqrt{\beta^2 - 4(1 - M^2 - P_e)}}{2}} + \frac{1}{\frac{\beta \pm \sqrt{\beta^2 - 4(1 - M^2 - P_e)}}{2}} \exp\left(-\frac{\beta \pm \sqrt{\beta^2 - 4(1 - M^2 - P_e)}}{2} \eta\right) \tag{13}$$

$$f'(\eta) = -\exp\left(-\frac{\beta \pm \sqrt{\beta^2 - 4(1 - M^2 - P_e)}}{2} \eta\right) \tag{14}$$

3. Flow Stability Analysis

To investigate the stability of the both (upper and lower) branches, we consider the unsteady version of Eqns. (2)-(4):

$$\frac{\partial \tilde{u}}{\partial t} + \tilde{u} \frac{\partial \tilde{u}}{\partial \tilde{x}} + \tilde{v} \frac{\partial \tilde{u}}{\partial \tilde{y}} = \nu_{nf} \frac{\partial^2 \tilde{u}}{\partial \tilde{y}^2} - \left(\frac{\sigma_{nf} B^2}{\rho_{nf}} + \frac{\mu_e}{\rho_{nf} k_e} \right) \tilde{u} \tag{15}$$

$$(\rho c)_{nf} \left(\frac{\partial \tilde{T}}{\partial t} + \tilde{u} \frac{\partial \tilde{T}}{\partial \tilde{x}} + \tilde{v} \frac{\partial \tilde{T}}{\partial \tilde{y}} \right) = k_{nf} \frac{\partial^2 \tilde{T}}{\partial \tilde{y}^2} + (\rho c)_p \left(D_B \left(\frac{\partial \tilde{C}}{\partial \tilde{y}} \right) + \frac{D_T}{T_\infty} \left(\frac{\partial \tilde{T}}{\partial \tilde{y}} \right) \right) \left(\frac{\partial \tilde{T}}{\partial \tilde{y}} \right) + \frac{\mu_e}{k_e} \tilde{u}^2 + \mu_{nf} \left[\frac{\partial \tilde{u}}{\partial \tilde{y}} \right]^2 \tag{16}$$

$$\frac{\partial \tilde{C}}{\partial t} + \tilde{u} \frac{\partial \tilde{C}}{\partial \tilde{x}} + \tilde{v} \frac{\partial \tilde{C}}{\partial \tilde{y}} = D_B \frac{\partial^2 \tilde{C}}{\partial \tilde{y}^2} + \frac{D_T}{T_\infty} \frac{\partial^2 \tilde{T}}{\partial \tilde{y}^2} \tag{17}$$

where t denotes the time. Introducing new similarity variables as follows:

$$\eta = \sqrt{\frac{a}{\nu_{nf}}} \tilde{y}, \quad u = a \tilde{x} \frac{\partial}{\partial \eta} f(\eta, \tau), \quad v = -\sqrt{a \nu_{nf}} f(\eta, \tau), \quad \tau = at, \quad \theta(\eta, \tau) = \frac{\tilde{T} - \tilde{T}_\infty}{\tilde{T}_w - \tilde{T}_\infty}, \quad \phi(\eta, \tau) = \frac{\tilde{C} - \tilde{C}_\infty}{\tilde{C}_\infty} \tag{18}$$

It follows that Eqns. (15)-(17) can be written as:

$$\frac{\partial^3 f}{\partial \eta^3} + f \frac{\partial^2 f}{\partial \eta^2} - \left(\frac{\partial f}{\partial \eta} \right)^2 - (M^2 + P_e) \frac{\partial f}{\partial \eta} - \frac{\partial^2 f}{\partial \tau \partial \eta} = 0 \tag{19}$$

$$\frac{\partial^2 \theta}{\partial \eta^2} + Nb \frac{\partial \theta}{\partial \eta} \frac{\partial \phi}{\partial \eta} + Nt \left(\frac{\partial \theta}{\partial \eta} \right)^2 + Pr \left[Ec \left\{ \left(\frac{\partial^2 f}{\partial \eta^2} \right)^2 + P_e \left(\frac{\partial f}{\partial \eta} \right)^2 \right\} + f \frac{\partial \theta}{\partial \eta} - 2 \frac{\partial f}{\partial \eta} \theta - \frac{\partial \theta}{\partial \tau} \right] = 0 \tag{20}$$

$$\frac{\partial^2 \phi}{\partial \eta^2} + Sc f \frac{\partial \phi}{\partial \eta} + \frac{Nt}{Nb} \frac{\partial^2 \theta}{\partial \eta^2} - \frac{\partial \phi}{\partial \tau} = 0 \tag{21}$$

The associated transformed boundary conditions are:

$$f(0, \tau) = \beta, \quad \frac{\partial f}{\partial \eta}(0, \tau) = \chi + \lambda \frac{\partial^2 f}{\partial \eta^2}(0, \tau), \quad \theta(0, \tau) = 1 + \delta \frac{\partial \theta}{\partial \eta}(0, \tau), \quad Nb \frac{\partial \phi}{\partial \eta}(0, \tau) + Nt \frac{\partial \theta}{\partial \eta}(0, \tau) = 0 \tag{22}$$

$$\text{as } \eta \rightarrow \infty, \quad \frac{\partial f}{\partial \eta}(\eta, \tau) = 0, \quad \theta(\eta, \tau) = 0, \quad \phi(\eta, \tau) = 0.$$

To test the stability of the steady flow solution satisfying the bvp (7)-(9), we write, following [18], [21]:

$$X(\eta, \tau) = X_0(\eta) + e^{-\alpha \tau} Y(\eta, \tau) \tag{23}$$

where $Y = P, Q$ and R are small disturbances relative to $X_0 = f_0, \theta_0$ and ϕ_0 , respectively and α is eigenvalue. Substituting Eqn. (23) into Eqns. (19)-(22), we obtain the following *linearized* eigenvalue problem:

$$P_0''' + f_0' P_0 + f_0 P_0'' - 2 f_0' P_0' - (M^2 + P_e) P_0' + \alpha P_0' = 0 \tag{24}$$

$$\frac{1}{Pr} [Q_0'' + Nb(\phi_0' Q_0' + \theta_0' R_0') + 2 Nt \theta_0' Q_0'] + f_0 Q_0' + \theta_0' P_0 - 2 \theta_0 P_0' - 2 f_0' Q_0 + Ec [2 f_0' P_0'' + 2 P_e f_0' P_0'] + \alpha Q_0 = 0, \tag{25}$$

$$R_0'' + Sc(\phi_0' P_0 + f_0 R_0') + \frac{Nt}{Nb} Q_0'' + \alpha R_0 = 0 \tag{26}$$



The corresponding boundary conditions:

$$\begin{aligned}
 P_0(0) = 0, \quad P_0'(0) = \lambda P_0''(0), \quad Q_0(0) = \delta Q_0'(0), \quad NbR_0'(0) + NtQ_0'(0) = 0 \\
 \text{as } \eta \rightarrow \infty, \quad P_0'(\eta) = 0, \quad Q_0(\eta) = 0, \quad R_0(\eta) = 0,
 \end{aligned}
 \tag{27}$$

4. Numerical Results and Discussion

The influence of governing parameters on skin friction $f''(0)$ and the rate of heat transfer at the surface $\{-\theta'(0)\}$ are investigated and numerical results [24] are tabulated and presented graphically. The default values of involving parameters are taken as $\chi = -1$ (shrinking case), $M = 0.1$ (for low magnetic field, $\ll 1$ Tesla), $Ec = 0.01$ (this value is generally very low for boundary layer flow), $\beta = 3.0$ (high value of suction parameter), $Pr = 6.8$ (water-based nanofluid), $Sc = 10$ (generally $\gg 1$ for nanofluid), $Nb = Nt = 0.1$ (value is very less for different nanofluid), $\lambda = 0.1$ (boundary layer slip), $\delta = 0.1$ (thermal slip) and $P_e = 0.01$ (the permeability parameter value is very low). Since dual solutions are considered, therefore solid and dashed lines represent the first and second solution respectively. The numerical results of flow equation for shrinking sheet have been compared with the exact analytical results of Fang and Zhang [4] in Table 1 and the result follows a certain relation (First solution + Second solution = value of suction). In order to verify the results of the thermal equation $\{-\theta'(0)\}$, the limiting case is compared with the refs. [44, 45] in Table 2 and a good agreement is reported. We have determined the smallest eigenvalues α for eigenvalue (EV) problem (Eqs. 24-27) for some values of the thermophysical parameters and results are documented in Table 3 predicts the stable behavior for the upper branch. The numerical results of the local Nusselt number are calculated and presented in Table 4. The different range of numerical values in Table 5, has been explored for both the branches of solution for different sets of slip parameters which also reveals the considerable dependence of Nusselt number (Heat Transfer) on Eckert number. The simple linear multiple regression estimations Nur_E of the Nusselt number is obtained using *LinearModel.fit* package in MATLAB considering the impact of velocity slip λ , thermal slip δ , Brownian motion parameter Nb and thermophoresis parameter Nt . Using a total of 576 observations ($\lambda = \delta = 0.05(0.05)0.2, Nb=Nt=0.05(0.05)0.3$), the linear regression estimations can be as $Nur_E = Nur + C_L\lambda + C_D\delta + C_B Nb + C_T Nt$ keeping default values of other parameters. The coefficients of Nur_E are shown in Table 6 which shows the dominant behavior of thermal slip. Thus, the suitable values of controlling parameters play a key role to understand the transport phenomena in current porous media model. Heat transfer (Nusselt number) is independent of the Nb and a decreasing function of all the other controlling parameters.

Table 1. Comparison of $f''(0)$ for shrinking ($\chi = -1$) sheet flow equation (without slip and nanoparticles)

		Exact Solution (Fang and Zhang [4])		Present result	
β	M	First	Second	First	Second
3.0	0.1	2.622497	0.377503	2.622497	0.377503
	0.5	2.724744	0.275255	2.724744	0.275256
	1	3.000000	0	3.000000	0
3.5	0.1	3.189618	0.310382	3.189618	0.310382
	0.5	3.270691	0.229309	3.270691	0.229309
	1	3.500000	0	3.500000	0

Table 2. Values of $\{-\theta'(0)\}$ for various values of Pr with $\lambda = \delta = P_e = Ec = Sc = \beta = M = 0, \chi = 1, Nb = Nt = 10^{-6}$.

Pr	Chen [44]	Khader and Megahed [45]	Present Result
0.72	1.08853	1.088487	1.088524
1.0	1.33334	1.333189	1.333333
3.0	2.50972	2.509201	2.509725
10.0	4.79686	4.794399	4.796863

Table 3. Smallest eigenvalues for the upper and lower branch for other default parameters

	β	Upper branch	Lower branch
$\lambda = 0.1$	3.0000	0.9565	-0.8348
	2.0500	0.5202	-0.4114
	1.9486	0.3000	-0.2630
	1.8893	0.0236	-0.0233
$\lambda = 0.2$	3.0000	0.9365	-0.8421
	2.0500	0.4968	-0.4768
	1.8232	0.1187	-0.1125
	1.8129	0.0139	-0.0138



Table 4. Numerical results of $(\{-\theta'(0)\})$ for the upper and lower branch with default values

Nt	P_e	$\{-\theta'(0)\}$	
		Upper branch	Lower branch
0.10	0.001	6.585995	6.525016
	0.01	6.585998	6.514861
	0.05	6.586001	6.349962
0.05		6.597811	6.526901
0.10	0.01	6.585998	6.514861
0.30		6.537769	6.465680

Table 5. Numerical results for heat transfer $(\{-\theta'(0)\})$ for different values of slip parameters.

λ	δ	$Ec=0.0001$		$Ec=0.01$	
		Upper Branch	Lower Branch	Upper Branch	Lower Branch
0	0	18.867346	18.743265	18.771104	18.577777
0	0.1	6.582183	6.567448	6.548162	6.507984
0	0.2	3.972842	3.967470	3.952321	3.931482
0.1	0	18.781777	18.781777	18.622525	18.622525
0.1	0.1	6.606917	6.572011	6.585997	6.514860
0.1	0.2	3.981773	3.969121	3.969174	3.934543
0.2	0	19.216928	18.815031	19.176971	18.660808
0.2	0.1	6.622846	6.575940	6.608899	6.520655
0.2	0.2	3.987502	3.970543	3.979111	3.937101

Table 6. Coefficients in Nur_E for default set of other parameters

Pr	Nur	C_L	C_D	C_B	C_T	RMSE (ϵ)	Adjusted R^2
1	2.2959	0.6406	-3.2907	-0.0000	-0.5832	0.022	0.987
5	9.1229	-0.1085	-28.4184	-0.0036	-0.3822	0.357	0.952
6.8	11.0802	0.2684	-37.9973	-0.0000	-0.2973	0.564	0.934
10	13.2495	-0.0331	-48.3577	-0.0180	-0.1517	0.806	0.918

4.1. Effect of velocity slip and suction parameter

The partial slip in the nanofluid flow regime has its own importance due to nanoparticle fluid interaction. The suction parameter sometimes plays a significant role in controlling the heat transfer, thus the impact of these parameters has been explored. Figure 2 illustrates the influence of the velocity slip parameter ($\lambda = L_1 \sqrt{a / \nu_{nf}}$), on the branches of the solution for stream function. Increasing velocity slip evidently enhances the upper branch solution whereas it diminishes the lower branch solution. Therefore in the absence of velocity (hydrodynamic wall) slip, the upper branch solution is minimized whereas the lower branch solution is maximized for this case. Generally, the upper branch solution exhibits a much steeper gradient near the sheet surface which is smoothed into a plateau as we progress into the boundary layer. The lower branch solution profiles at all velocity slip values are generally monotonic growths from a minimum at the wall (sheet surface) to a maximum in the free stream. Figure 3 depicts the collective effect of velocity slip parameter (λ) and mass transfer parameter (β) i.e. suction parameter on skin friction profiles. It is evident that the mass transfer parameter exerts a substantial influence on the existence of dual solutions. With an increase in the velocity slip parameter, both upper and lower branch solutions are decreased. These trends confirm that the wall skin friction is reduced with increasing hydrodynamic slip at the wall. The values of β_c , critical points (turning points) are also decreased from 1.9794 to 1.8182 with the variation of the velocity slip parameter from 0 to 0.2. Beyond the critical points, no solution exists. Even the velocity slip parameter has some impact on heat transfer, which slightly suppresses its value from 5.2319 to 5.1355 (Nearly 1% reduction) shown in Fig. 4.

4.2. Effect of Eckert number and nanofluid parameter (Nt)

The dissipation due to the flow model does play a significant role which can't be neglected in the case of nanoparticles. From the regression analysis, we can interpret the insignificance of Brownian motion towards heat transfer management. So, we have studied the collective influence of Eckert number (Ec) and thermophoresis parameter (Nt) on the temperature evolution in the boundary layer (shown in Fig. 5). Both parameters generally enhance temperature values. Eckert number embodies the quantity of mechanical energy converted to heat via viscous dissipation. The supplementary thermal energy generated clearly heats the boundary layer and enhances temperatures and will also elevate thermal boundary layer thickness. The thermophoresis parameter quantifies the intensity of the thermophoretic migration of nanoparticles. With increasing values of this parameter, thermal diffusion is encouraged in the regime and energizes the flow. In all cases, the temperature profiles exhibit monotonic decay from the wall to the free stream and the variation in values at the wall ($\eta=0$) is associated with the non-isothermal conditions prescribed there.



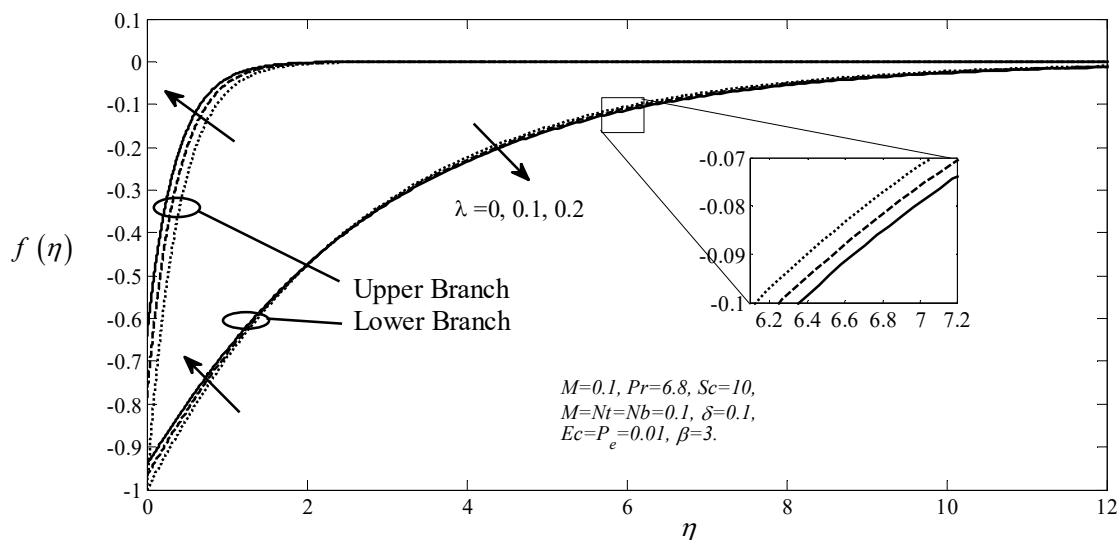


Fig. 2. Upper and lower branches of stream function profiles with different velocity slip.

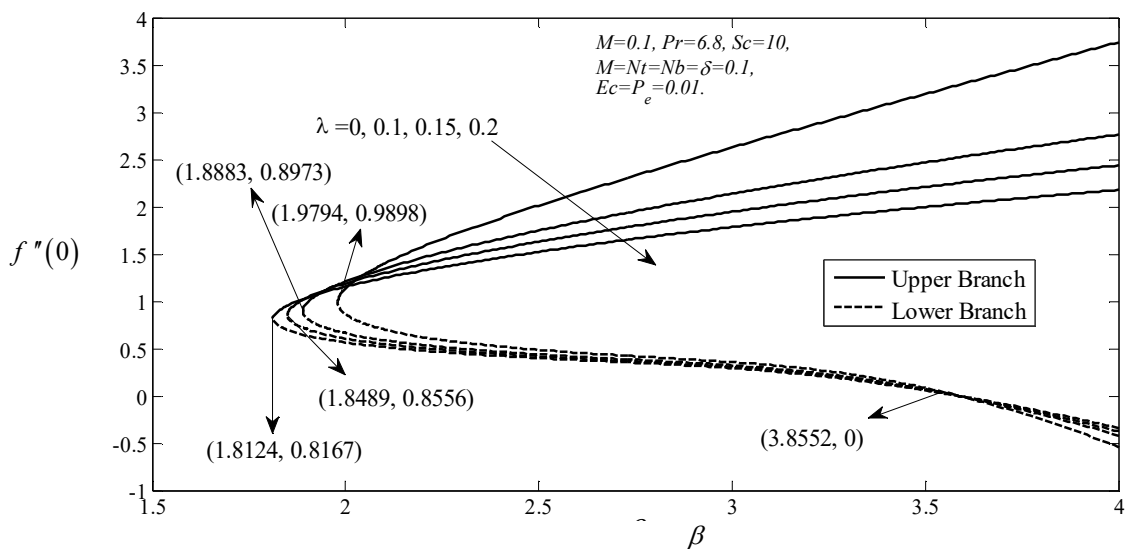


Fig. 3. Variation of skin friction $f''(0)$ with mass transfer parameter β and velocity slip parameter λ .

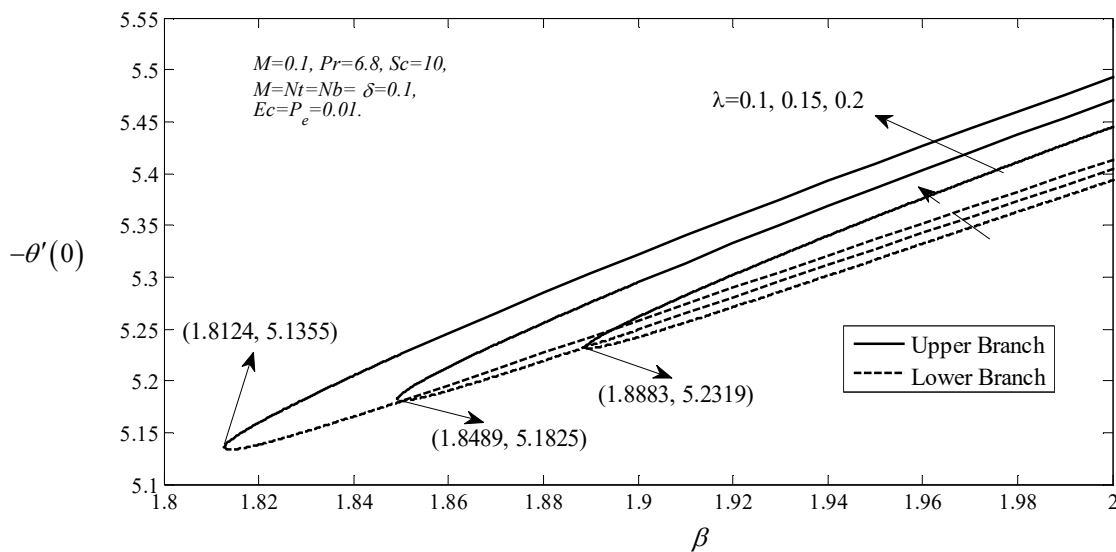


Fig. 4. The effects of velocity slip parameter λ and mass transfer parameter β on the rate of heat transfer at the surface $\{-\theta'(0)\}$.

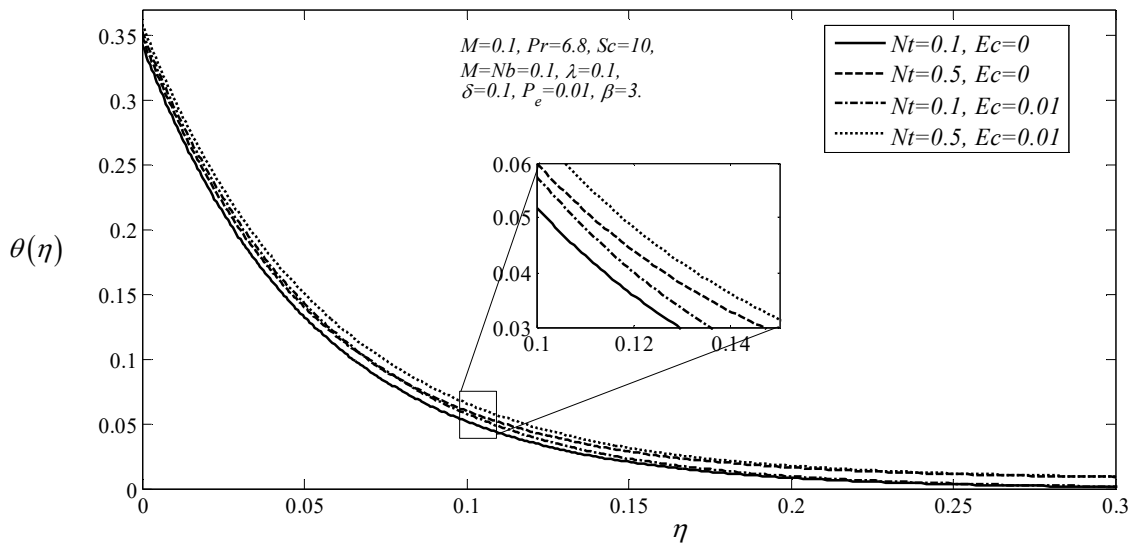


Fig. 5. Temperature distribution for different values of Ec and Nt for the upper branch.

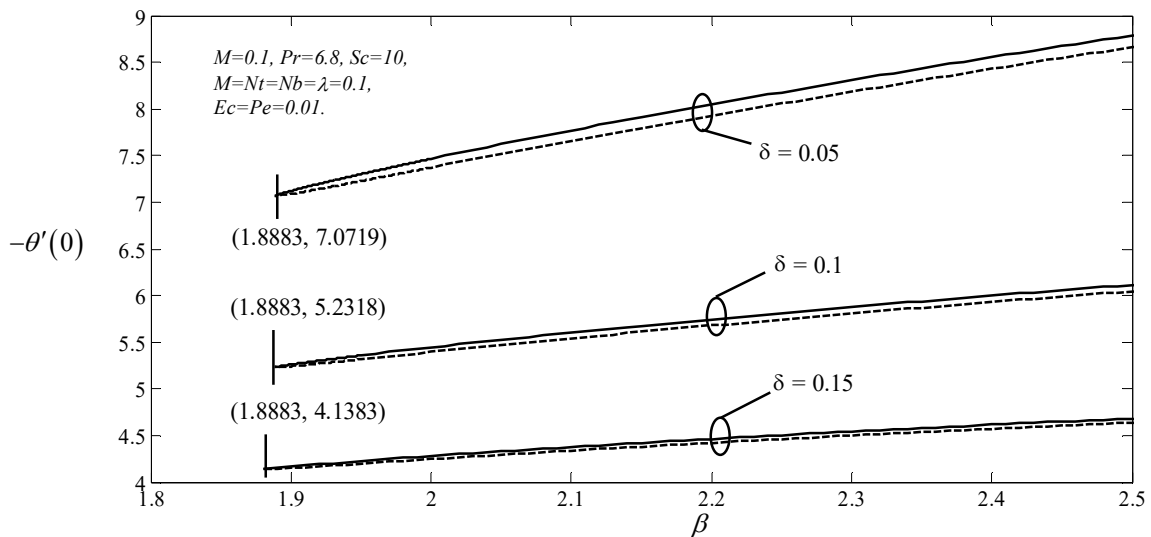


Fig. 6. The effects of thermal slip parameter δ and mass transfer parameter s on the rate of heat transfer at the surface $\{-\theta'(0)\}$.

4.3. Effect of thermal slip and suction parameters

The thermal slip parameter is required to properly analyze the realistic situation for heat transfer as the nanoparticles can be used as a controlling agent for many industrial applications. Figure 6 depicts the collective effect of thermal slip parameter, δ and mass transfer parameter, β on the rate of heat transfer at the surface $\{-\theta'(0)\}$. With greater thermal slip (thermal jump at the wall) the surface heat transfer rate is consistently decreased. The upper branch solution always exceeds the lower branch solution. With increasing suction ($\beta > 0$) both upper and lower branch solutions for heat transfer rate are generally elevated. The deceleration in the flow with suction effectively boosts heat transfer to the wall i.e. cools the boundary layer. The wall (sheet surface) is therefore cooled significantly as thermal slip increases (with associated heating of the nanofluid and greater thermal boundary layer thickness). Obviously, thermal slip consideration along with backflow arises due to shrinking sheet, can significantly change the heat transfer.

4.4. Effect of permeability and magnetic parameter

There are many applications related to the nanoparticle flow in porous media that require a detailed analysis of convective heat transfer. The porous media slows down the flow thus have high impact on heat transfer along with Lorentz force due to electrical conducting behavior of nanofluid (ions are the carriers). Even the permeability parameter plays a crucial role while dealing with nanoparticles. Thus, Fig. 7 depicts the variation in heat transfer with permeability parameter, P_e , Magnetic parameter (M) which respect to mass transfer parameter. The correct response is therefore associated with the lower branch since greater permeability parameter (inversely proportional to regime permeability) leads to an increase in Darcian body force (porous media impedance) in the regime and this decelerates the flow



manifesting with lower heat transfer. With increasing magnetic parameter (retarding force), there is an increment in Nusselt number for the upper branch solution whereas there is a decrement in the lower branch solution for Nusselt number. Generally, both solutions are quite sensitive to modification in the permeability parameter and Magnetic parameter. The streamline patterns are shown for different cases of stretching ($\beta = 0$) and shrinking ($\beta = 3$) parameters for default set of parameter in Fig. 8. The lower branch (unstable) shows the abrupt behavior due to higher value of suction which changes the flow motion. The impact is more pronounced with the utilization of nanoparticles.

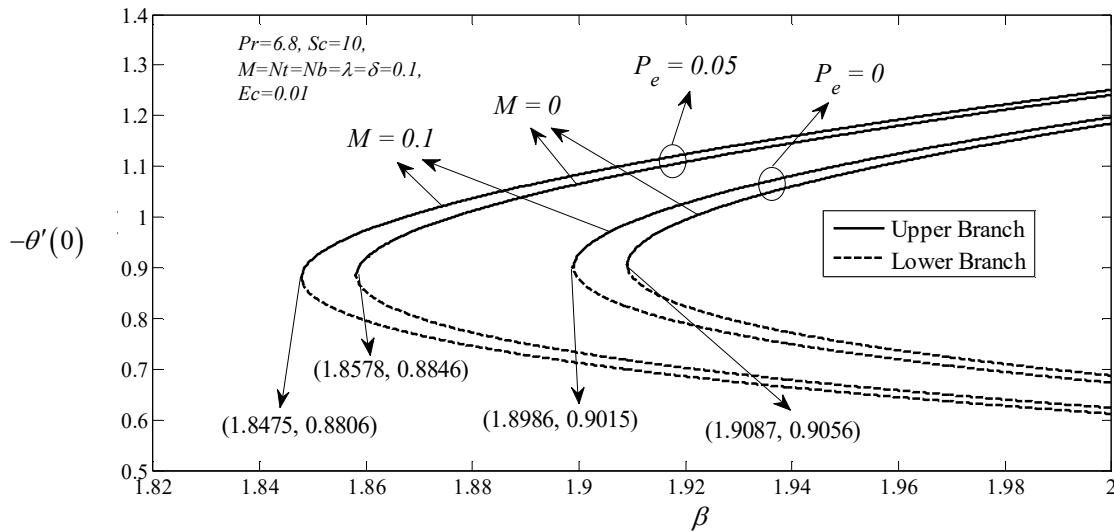
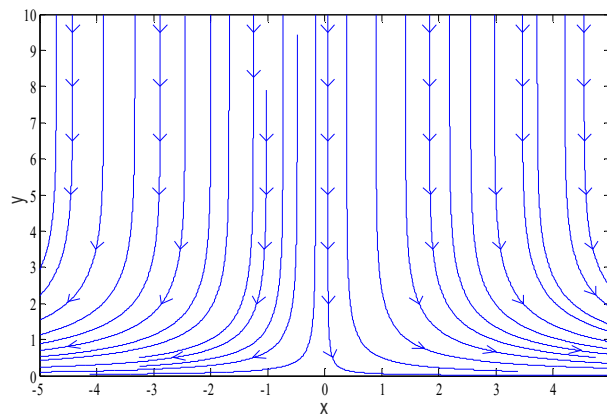
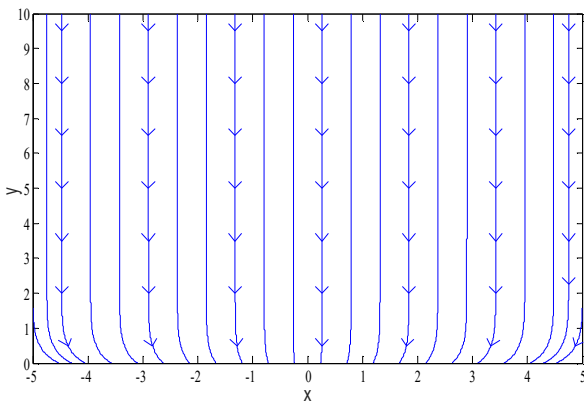


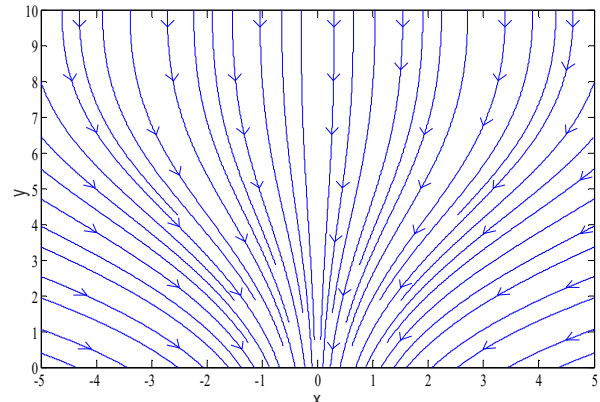
Fig. 7. Variation of heat $\{-\theta'(0)\}$ with permeability parameter P_e and Magnetic field parameter (M).



(a) Streamlines
(Stretching Sheet, $\beta = 0$)



(b) Streamlines Upper Branch
(Shrinking Sheet, $\beta = 3$)



(c) Streamlines Lower Branch
(Shrinking Sheet, $\beta = 3$)

Fig. 8. Streamlines for the default set of parameter otherwise stated on the caption

5. Concluding Remarks

The effects of velocity slip, thermal slip and permeability of porous medium on time-dependent magneto-hydrodynamic over a permeable shrinking sheet have been studied numerically utilizing nanoparticles. A stability analysis is performed on the unsteady version of the transformed equations, and eigenvalues are determined to correspond to stable and unstable solutions. The main findings are listed below:

1. An adequate suction is required at the surface for the existence of both solutions. In the case of a shrinking sheet, the solution may not exist without the suction parameter.
2. The range of solution is increased by applying slip (velocity) condition but the imposition of thermal slip does not improve the range. Thus, the assumption of partial slip entirely changes the transport phenomena in nanofluids.
3. The stability analysis has demonstrated that the first solution is stable and thus physically reliable, while the second solution is not.
4. Skin friction is lower for the velocity slip condition and the wall rate of heat transfer is higher for larger values of the suction parameter in the absence of the thermal slip condition. The application of suction leads to enhancement of wall friction as well as heat transfer for the stable branch.
5. Magnetic field (Lorentz force) and permeability parameter both enhances the heat transfer in nanofluids for stable (realizable branch).
6. Multiple regression estimation (MRE) predicts the impact of important parameters on Nusselt number which shows the insignificance of Brownian motion.

Author Contributions

Y. Gupta planned and initiated the project and suggested the appropriate mathematical model for present nanofluid problem. P. Rana performed the stability analysis and developed the MATLAB codes. O. Anwar Bég conducted the numerical experiments and examined the validation of result. The manuscript was written through the contribution of all authors. All authors discussed the results, reviewed and approved the final version of the manuscript.

Conflict of Interest

The authors declared no potential conflicts of interest with respect to the research, authorship and publication of this article.

Funding

The authors received no financial support for the research, authorship and publication of this article.

References

- [1] Crane L.J., Flow past a stretching plate, *Applied Mathematics and Physics*, 21, 1970, 645-647.
- [2] Miklavcic M., Wang C.Y., Viscous flow due to a shrinking sheet, *Quarterly of Applied Mathematics*, 64, 2006, 283-290.
- [3] Fang T, Boundary layer flow over a shrinking sheet with power-law velocity, *International Journal of Heat and Mass Transfer*, 51, 2008, 5838-5843.
- [4] Fang T., Zhang J., Closed-form exact solution of MHD viscous flow over a shrinking sheet, *Communications in Nonlinear Science and Numerical Simulation*, 14, 2009, 2853-2857.
- [5] Javed T., Abbas Z., Sajid M., Ali N., Heat transfer analysis for a hydromagnetic viscous fluid over a non-linear shrinking sheet, *International Journal of Heat and Mass Transfer*, 54, 2011, 2034-2042.
- [6] Buongiorno J., Convective transport in nanofluids, *ASME Journal of Heat Transfer*, 128, 2006, 240-250.
- [7] Rohni A.M., Ahmad S., A., Ismail A. I. Md., Pop I., Flow and heat transfer over an unsteady shrinking sheet with suction in a nanofluid using Buongiorno's model, *International Communications in Heat and Mass Transfer*, 43, 2013, 75-80.
- [8] Zaimi K., Ishak A., Pop I., Flow past a permeable stretching/shrinking sheet in a nanofluid using two-phase model, *Plos One*, 9, 2014, 111743 (1-6).
- [9] Naramgari S., Sulochana C., MHD flow over a permeable stretching/shrinking sheet of a nanofluid with suction/injection, *Alexandria Engineering Journal*, 55, 2016, 819-827.
- [10] Uddin Md.J., Bég O.Anwar and Ismail A.I., Radiative convective nanofluid flow past a stretching/shrinking sheet with slip effects, *AIAA Journal of Thermophysics and Heat Transfer*, 29, 2015, 513-523.
- [11] Singh G., Chamkha A.J., Dual solutions for second-order slip flow and heat transfer on a vertical permeable shrinking sheet, *Ain Shams Engineering Journal*, 4, 2013, 911-917.
- [12] Hsiao, K. L., To promote radiation electrical MHD activation energy thermal extrusion manufacturing system efficiency by using Carreau-Nanofluid with parameters control method, *Energy*, 130, 2017, 486-499.
- [13] Hsiao, K. L., Combined electrical MHD heat transfer thermal extrusion system using Maxwell fluid with radiative and viscous dissipation effects, *Applied Thermal Engineering*, 112, 2017, 1281-1288.
- [14] Hsiao, K. L., Micropolar nanofluid flow with MHD and viscous dissipation effects towards a stretching sheet with

- multimedia feature, *International Journal of Heat and Mass Transfer*, 112, 2017, 983-990.
- [15] Hsiao, K. L., Stagnation electrical MHD nanofluid mixed convection with slip boundary on a stretching sheet, *Applied Thermal Engineering*, 98, 2016, 850-861.
- [16] Waqas, M., Shehzad, S. A., Hayat, T., Khan, M. I., Alsaedi, A., Simulation of magnetohydrodynamics and radiative heat transport in convectively heated stratified flow of Jeffrey nanofluid, *Journal of Physics and Chemistry of Solids*, 133, 2019, 45-51.
- [17] Waqas, M., Jabeen, S., Hayat, T., Khan, M. I., Alsaedi, A., Modeling and analysis for magnetic dipole impact in nonlinear thermally radiating Carreau nanofluid flow subject to heat generation, *Journal of Magnetism and Magnetic Materials*, 485, 2019, 197-204.
- [18] Dhanai R., Rana P., Kumar L., MHD mixed convection nanofluid flow and heat transfer over an inclined cylinder due to velocity and thermal slip effects: Buongiorno's model, *Powder Technology*, 288, 2016, 140-150.
- [19] Subba Rao, A., V.R.Prasad, K. Harshavalli and O. Anwar Bég, Thermal radiation effects on non-Newtonian fluid in a variable porosity regime with partial slip, *Journal of Porous Media*, 19 (4), 2016, 1-17.
- [20] Siavashi, M., Karimi, K., Xiong, Q., Doranehgard, M. H., Numerical analysis of mixed convection of two-phase non-Newtonian nanofluid flow inside a partially porous square enclosure with a rotating cylinder, *Journal of Thermal Analysis and Calorimetry*, 137(1), 2019, 267-287.
- [21] Dhanai R., Rana P., Kumar L., Multiple solutions of MHD boundary layer flow and heat transfer behavior of nanofluids induced by a power-law stretching/shrinking permeable sheet with viscous dissipation, *Powder Technology*, 273, 2015, 62-70.
- [22] Izadi, A., Siavashi, M., Xiong, Q., Impingement jet hydrogen, air and CuH₂O nanofluid cooling of a hot surface covered by porous media with non-uniform input jet velocity, *International Journal of Hydrogen Energy*, 44(30), 2019, 15933-15948.
- [23] Bég, O. Anwar, M. F. M. Basir, M.J. Uddin and A. I. Md. Ismail, Numerical study of slip effects on asymmetric bioconvective nanofluid flow in a porous microchannel with an expanding/contracting upper wall using Buongiorno's model, *Journal of Mechanics in Medicine and Biology*, 17, 2017, 1750059.
- [24] Rashid, M., Khan, M. I., Hayat, T., Khan, M. I., Alsaedi, A., Entropy generation in flow of ferromagnetic liquid with nonlinear radiation and slip condition, *Journal of Molecular Liquids*, 276, 2019, 441-452.
- [25] Khan, M. W. A., Khan, M. I., Hayat, T., Alsaedi, A., Entropy generation minimization (EGM) of nanofluid flow by a thin moving needle with nonlinear thermal radiation, *Physica B: Condensed Matter*, 534, 2018, 113-119.
- [26] Shukla, N., Rana, P., Bég, O.A., Singh, B. and Kadir, A., Homotopy study of magnetohydrodynamic mixed convection nanofluid multiple slip flow and heat transfer from a vertical cylinder with entropy generation, *Propulsion and Power Research*, 8, 2019, 147-162.
- [27] Rana, P., Shukla, N., Bég, O.A. and Bhardwaj, A., Lie group analysis of nanofluid slip flow with Stefan Blowing effect via modified Buongiorno's Model: entropy generation analysis, *Differential Equations and Dynamical Systems*, 2019, 1-18.
- [28] Rana, P. and Shukla, N., Entropy generation analysis for non-similar analytical study of nanofluid flow and heat transfer under the influence of aligned magnetic field, *Alexandria Engineering Journal*, 57(4), 2018, 3299-3310.
- [29] Hayat, T., Khan, M. I., Farooq, M., Alsaedi, A., Waqas, M., Yasmeen, T., Impact of Cattaneo-Christov heat flux model in flow of variable thermal conductivity fluid over a variable thicked surface, *International Journal of Heat and Mass Transfer*, 99, 2016, 702-710.
- [30] Hayat, T., Khan, M. I., Farooq, M., Yasmeen, T., Alsaedi, A., Stagnation point flow with Cattaneo-Christov heat flux and homogeneous-heterogeneous reactions, *Journal of Molecular Liquids*, 220, 2016, 49-55.
- [31] Khan, M. I., Waqas, M., Hayat, T., Alsaedi, A., A comparative study of Casson fluid with homogeneous-heterogeneous reactions, *Journal of Colloid and Interface Science*, 498, 2017, 85-90.
- [32] Hayat, T., Aslam, N., Khan, M. I., Khan, M. I., Alsaedi, A., Physical significance of heat generation/absorption and Soret effects on peristalsis flow of pseudoplastic fluid in an inclined channel, *Journal of Molecular Liquids*, 275, 2019, 599-615.
- [33] Hayat, T., Javed, S., Khan, M. I., Khan, M. I., Alsaedi, A., Physical aspects of irreversibility in radiative flow of viscous material with cubic autocatalysis chemical reaction, *The European Physical Journal Plus*, 134(4), 2019, 172.
- [34] Ghosh S., Mukhopadhyay S., Vajravelu K., Dual solutions of slip flow past a nonlinearly shrinking permeable sheet, *Alexandria Engineering Journal*, 55, 2016, 1835-1840.
- [35] Rana P., Dhanai R., Kumar L., Radiative nanofluid flow and heat transfer over a non-linear permeable sheet with slip conditions and variable magnetic field: Dual solutions, *Ain Shams Engineering Journal*, 8, 2017, 341-352.
- [36] Merkin J.H., On dual solution occurring in mixed convection in a porous medium, *Journal of Engineering Mathematics*, 20, 1985, 171-179.
- [37] Harris S.D., Ingham D.B., Pop I., Mixed convection boundary layer flow near the stagnation point on a vertical surface in a porous medium: Brinkman model with slip, *Transport in Porous Media*, 77, 2009, 267-285.
- [38] Awaludin, I.S., Ishak, A. and Pop, I., 2018. On the stability of MHD boundary layer flow over a stretching/shrinking wedge, *Scientific Reports*, 8(1), 2018, 13622.
- [39] Yasin, M.H.M., Ishak, A. and Pop, I., Boundary layer flow and heat transfer past a permeable shrinking surface embedded in a porous medium with a second-order slip: A stability analysis, *Applied Thermal Engineering*, 115, 2017, 1407-1411.

- [40] Rana, P., Dhanai, R. and Kumar, L., 2017. MHD slip flow and heat transfer of Al₂O₃-water nanofluid over a horizontal shrinking cylinder using Buongiorno's model: Effect of nanolayer and nanoparticle diameter, *Advanced Powder Technology*, 28(7), 2017, 1727-1738.
- [41] Rana, P., Uddin, M.J., Gupta, Y. and Ismail, A.M., Slip effects on MHD Hiemenz stagnation point nanofluid flow and heat transfer along a nonlinearly shrinking sheet with induced magnetic field: multiple solutions, *Journal of the Brazilian Society of Mechanical Sciences and Engineering*, 39(9), 2017, 3363-3374.
- [42] Rana, P., Shukla, N., Gupta, Y. and Pop, I., 2019. Homotopy analysis method for predicting multiple solutions in the channel flow with stability analysis, *Communications in Nonlinear Science and Numerical Simulation*, 66, 2019, 183-193.
- [43] Rana, P., Shukla, N., Gupta, Y. and Pop, I. Analytical prediction of multiple solutions for MHD Jeffery–Hamel flow and heat transfer utilizing KKL nanofluid model, *Physics Letters A*, 383(2-3), 2019, 176-185.
- [44] Chen, C.H., Laminar mixed convection adjacent to vertical, continuously stretching sheets, *Heat and Mass Transfer*, 33, 1998, 471–476.
- [45] Khader, M. M., Megahed, A. M., Effect of viscous dissipation on the boundary layer flow and heat transfer past a permeable stretching surface embedded in a porous medium with a second-order slip using Chebyshev finite difference method, *Transport in Porous Media*, 105(3), 2014, 487-501.

ORCID iD

Yogesh Gupta  <https://orcid.org/0000-0002-9285-4526>

Puneet Rana  <https://orcid.org/0000-0002-9850-763X>



© 2020 by the authors. Licensee SCU, Ahvaz, Iran. This article is an open access article distributed under the terms and conditions of the Creative Commons Attribution-NonCommercial 4.0 International (CC BY-NC 4.0 license) (<http://creativecommons.org/licenses/by-nc/4.0/>).